Excited-State Ab Initio Calculations and Multidimensional Franck−Condon Simulations on Guanine

Igor Pugliesi* and Klaus Müller-Dethlefs†

York Centre of Laser Spectroscopy (YCLS), Department of Chemistry, The University of York, Heslington, York, YO10 5DD, United Kingdom

Received: April 24, 2006; In Final Form: August 22, 2006

The guanine enol and keto N7H and N9H tautomers have been optimized at the CASSCF/cc-pVDZ levels of theory. Except for the enol N7H tautomer, CASSCF predicts distorted nonplanar S_1 state geometries. Among the vibronic simulations carried out with the optimized structures only the enol N7H tautomer qualitatively mirrors the appearance of the experimental R2PI spectrum. Refined symmetry-adapted cluster configuration interaction (SACCI) geometries of the enol N7H tautomer produce simulations in good agreement with experiment and support the assignment of the first vibronic band and associated vibronic features of the R2PI spectrum to this tautomer. The sharp spectral features and the fact that Franck−Condon simulations based on the harmonic approximation allow for a faithful reproduction of the spectral signature associated with the enol N7H tautomer indicate that within the simulated energy window the S_1 potential energy surface of this isomer is fairly harmonic and free from conical intersections involved in the S_1 state lifetime-shortening relaxation processes of other DNA bases and possibly the remaining tautomers of guanine.

1. Introduction

Understanding the large biomolecules that make up cells and more complex life forms requires an in depth investigation of their smaller building blocks (amino acids and nucleic acid bases) through experiment and theory. Numerous spectroscopic investigations on laser-desorbed DNA bases and base pairs[1] have recently been conducted, and an extensive literature of vibronic spectra is now available. These studies reveal details of the conformational landscapes and potential energy surfaces. Interestingly it was observed that the size and complexity of a biomolecule actually leads to *simplification* of its conformational landscape. For example, when the spectra of single amino acids with those of di- and tripeptides are compared, it is apparent that the former are congested by contributions from several conformers of each amino acid, while only one or two are observed for the latter.[2] The same is true for nucleic acid bases and base pairs. In the case of guanine, at least four different tautomers have been observed in the R2PI spectrum, while only one species gives rise to the resonant two-photon ionization (R2PI) spectrum of the guanine−cytosine base pair.[3] Similar results have been found for the guanine[4] and cytosine dimers[5] as well as guanosine[6,7] and may be attributed at least in part to the highly specific monomer conformations required for RNA/DNA chain formation.

One complicating factor in spectroscopic studies of biomolecules is that even when a given spectrum clearly derives from a single structure (conformer or tautomer), it is not necessarily straightforward to reach an unambiguous assignment.[8] Spectral deconvolution strategies based on complementing spectroscopic techniques and ab initio calculations are often not sufficient to provide unambiguous assignments. Generally, it is the accurate knowledge of the first electronically excited singlet state that is a crucial factor in understanding the features of vibronic spectra, but ab initio calculations on excited states provide a considerable challenge. Despite the recent growth in the number of ab initio approaches for structural determination of excited states, many of these methods are computationally intensive, and it is often difficult, if not impossible, to apply them even to small biomolecules such as single amino acids or DNA bases. Thus, in many cases the geometry of the neutral ground state is assumed to be a good approximation to the excited-state geometry.

Spectroscopic experiments probe the potential energy surface; ab initio methods help describe it. Both worlds reveal something about structure, but they must be brought closer together for us to gain a clearer view. One way to achieve this is by extracting further information from the results of theoretical calculations. Vibronic transition intensities are extremely sensitive to the upper and lower state geometries and so are their theoretical counterparts, the Franck−Condon integrals. A spectral analysis based on Franck−Condon simulations of vibronic spectra would therefore confer the additional benefit of structurally related information. However, in order for such a strategy to work, the calculated structures used in the simulations must be of high quality. Schumm et al.[9] and Spangenberg et al.,[10] for example, demonstrated that in the case of phenol, the CASSCF geometries are not accurate enough to generate Franck−Condon simulations faithful to experiment. The multidimensional Franck−Condon studies on phenol and phenol−nitrogen by Pugliesi and coworkers[11,12] were the first that directly compared S_0 and S_1 equilibrium geometries generated from different ab initio methods (specifically CASSCF, MRCI, and SACCI). They revealed that refining CASSCF equilibrium structures with the SACCI ab initio method results in geometries that generally allow for simulations that are much closer to experiment than CASSCF and have suggested that the above strategy could be a powerful tool for spectral assignment and deconvolution.

* Corresponding author. E-mail: igor.pugliesi@gmail.com.

† Current address: The Photon Science Institute, Simon Building, The University of Manchester, Manchester, M13 9PL, United Kingdom. E-mail: k.muller-dethlefs@manchester.ac.uk. Phone: +44 (0)161 275 1000.

10.1021/jp062494d CCC: $33.50
Published on Web 11/10/2006

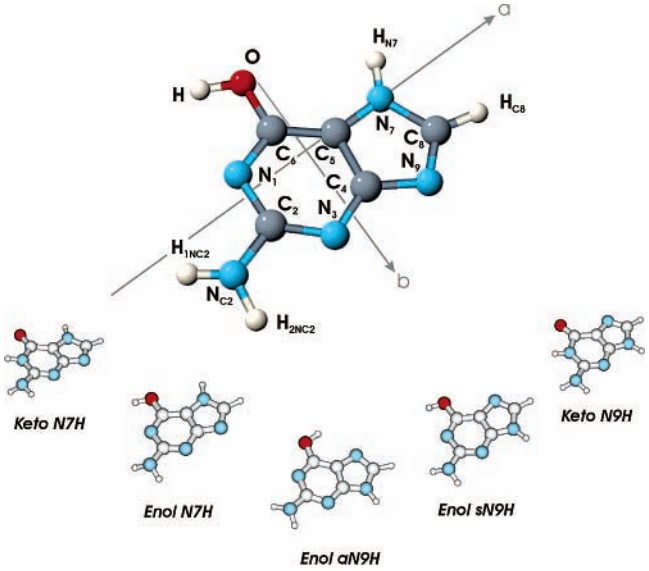

Figure 1. Atom labels for the enol N7H tautomer and structures of the four most stable tautomers of guanine including the anti (a) and syn (s) rotamers for enol N9H.

R2PI spectra of laser-desorbed guanine have recently been recorded by Nir et al.[13] and Piuzzi et al.[14] The authors identified contributions from up to four different tautomers in the observed spectrum: these comprise the N7H and N9H enol and the N7H and N9H keto forms (Figure 1). Nir et al. assigned the first origin band in the spectrum (band A) to the N9H enol tautomer based on the similarity of MP2 S_0 and CIS S_1 frequencies to the S_1 experimental frequencies. From their study, it is clear that none of the keto forms can be associated with band A as the R2PI spectrum of 1-methylguanine, which cannot form an enol tautomer, does not bear any similarities with the spectrum of guanine. The IR−UV depletion study on the guanine 7- and 9-methylated derivatives carried out by Mons et al.[15] confirm an assignment of band A to an enol form, but they suggested that it is due to the enol N7H and not the N9H tautomer.

The first ab initio calculations on the excited states of guanine were carried out by Petke et al.[16] By using the random phase approximation (RPA) and MRCI and by assuming planar geometries based on experimental data they calculated vertical transition energies to several electronic states of the keto tautomers. CASSCF and CASPT2 vertical transition energies of the keto N9H tautomer were performed by Fulscher et al.,[17] who also assumed the geometry to be planar. Full geometry optimizations and frequencies on the excited states of both enol and keto tautomers using the restricted open shell Kohn−Sham (ROKS) method have been carried out by Langer and Doltsinis[18] The relative tautomer transition energies found in all of these studies are in disagreement with the experimental assignments by Nir et al. and Mons et al. insofar as they all suggest that the keto N7H tautomer has the lowest transition energy.

Clearly spectral assignments based on transition energies can be misleading. Inspection of the predicted S_0-S_1 induced geometry changes and, where possible, Franck−Condon simulations based on the theoretical equilibrium geometries could shed more light onto the electronic spectra of guanine and, furthermore, give direct information about the structure of the first singlet excited state of the individual tautomers.

In this paper, we therefore present CIS and, for the first time, a complete CASSCF study including optimized geometries and frequencies on both the enol and keto tautomers of guanine as well as SACCI calculations on the enol N7H tautomer. The S_0 and S_1 equilibrium geometries thus obtained are used to generate Franck−Condon simulations of the tautomer-specific R2PI spectra, and an interpretation of the complete R2PI spectrum of guanine will be attempted on the basis of these simulations. In the analysis that follows, we adopt the convention introduced by Mons et al.[15] and label in order of ascending energy the origin bands associated with the four guanine tautomers as A, B, C, and D.

Franck−Condon simulations of the vibronic spectra of guanine analogues—the fluorescence spectra of indole by Callis et al.[19] and recently the R2PI spectra of 9H- and 7H-2-aminopurine[20] (in the Supporting Information)—have been carried out before, yet the ab initio wave functions used to obtain equilibrium structures and frequencies were not as highly correlated as the ones employed in this study.

The code used for the simulations has been described in a previous paper.[11] Briefly, it is based on the method of Doktorov et al.,[21] which is exact within the harmonic approximation and includes multidimensional potential surface displacements, mode frequency changes upon excitation, and mode mixing (Duschinsky rotations).

2. Ab Initio Methodologies

HF/CIS Calculations. HF/cc-pVDZ calculations have been carried out for the enol and keto N7H and N9H tautomers to generate optimized structures and frequencies for the neutral ground state. Similarly, for the S_1 state, CIS/cc-pVDZ equilibrium geometries and harmonic frequencies have been obtained.

CASSCF Calculations. CASSCF/cc-pVDZ calculations have been carried out for the enol and keto N7H and N9H tautomers to generate optimized structures and frequencies of the S_0, S_1, and D_0 states. Natural populations of the active space orbitals and harmonic frequencies are listed in Tables S1−S4 in the Supporting Information. For the enol tautomers, an active space consisting of 14 electrons distributed among 11 orbitals was employed (see Figure 2). It comprised the eight π orbitals delocalized on the aromatic ring and three more localized orbitals centered on the oxygen (p_π^O) and the two amines N_{C2} (p_π^{NC2}) and N_7/N_9 ($p_\pi^{N7/9}$). In the case of the keto tautomers, the study on the cytosine keto form by Ismail et al.[22] has been used as a guide. As with cytosine, convergence of a pure S_1 state wave function was not achievable, which is almost certainly due to the fact that at the level of theory used the S_1 global minimum structure coincides with the S_0/S_1 conical intersection. To avoid this problem, state averaging was employed, as this allows for the generation of orthonormal and thus noninteracting S_0 and S_1 wave functions solving the root-flipping problems occurring close to conical intersections. The S_1 and S_0 state CASSCF wave functions were mixed with a 1:1 weighting. The geometry of the S_1 state was optimized and frequencies and natural orbitals obtained as the second root of the state-averaged CASSCF wave function. For the ground-state geometry optimization and frequencies a pure S_0 CASSCF wave function was used. Convergence issues in the S_1 state required the CASSCF wave function to be generated from a smaller active space (10,9) than the one used for the enol tautomers (14,11). It consisted of the eight π orbitals delocalized on the aromatic ring and a more localized p_π orbital centered on the N_9 amine group. A p_π^O orbital was implicitly included with the ring π orbitals as the keto oxygen interacts with the aromatic ring system more strongly than the enol oxygen. The only major difference between the active spaces of the enol and keto tautomers was thus the exclusion of the orbital localized on the N_{C2} amine, which is arguably not important to this study.

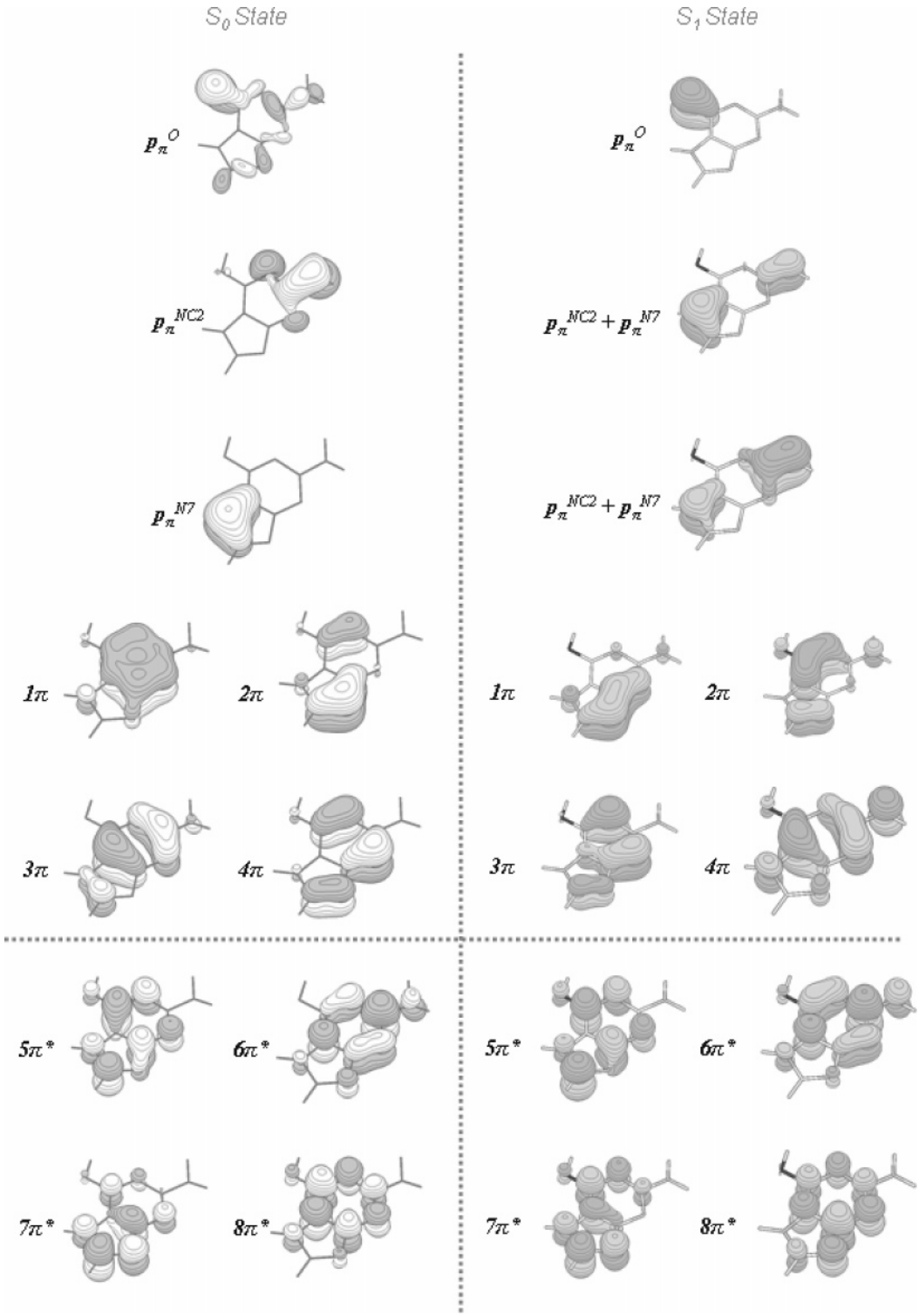

Figure 2. (14,11)-CASSCF/cc-pVDZ natural orbitals of the enol N7H tautomer. The natural orbitals of the enol N9H and the keto N7H and N9H tautomers are similar but with differing positions of the nodal planes.

SACCI Calculations. For reasons that will be explained in later sections of this paper, SACCI/cc-pVDZ geometry optimizations of the S_0 and S_1 states have only been performed on the enol N7H tautomer. All coordinates were optimized following analytic gradients. For calculation efficiency the S_0 CASSCF/cc-pVDZ equilibrium structure was used as starting geometry. All single-excitation operators were included in the linked terms, and the full valence space was used as active space. A level two perturbation selection was carried out for the linked double-excitation operators. No R2S2-type unlinked operators were included in the SACCI wave function. This led to an excitation space of 52820 operators for the SAC and 54657 operators for the S_1 state SACCI wave functions. The geometries obtained after three macroiterations were used for the Franck−Condon simulations. To obtain frequencies and normal modes, a strategy similar to the one employed for phenol in ref 11 was used. S_0 and S_1 frequencies were determined at the (8,8)-CASSCF/cc-pVDZ level of theory. The (8,8) active space consisted of the last eight orbitals shown in Figure 2. With a natural population of 1.99 and thus a very small multireference character, the first three orbitals in Figure 2 were excluded. The normal-mode analyses yielded no negative frequencies but large

TABLE 1: Relative Energies, S_0–S_1 Transition Energies, and Adiabatic Ionization Potentials of Guanine Tautomers in the Gas Phase

	enol N7H	enol sN9H	enol aN9H	keto N7H	keto N9H
Relative Energies Including ZPE Corrections/kJ mol^{-1}					
CASSCF/cc-pVDZ[a]					
S_0	29.66	14.80	18.56	3.14	0.00
S_1	0.00	12.69	11.06		
D_0	49.03	31.43	38.33	17.89	0.00
CASSCF/cc-pVDZ[b]					
S_0				2.58	0.00
S_1	92.85	105.02	106.90	136.21	0.00
D_0					
CIS/cc-pVDZ					
S_1	20.85	31.66	34.86	0.00	1.94
RI-MP2/TZVPP[c]					
S_0	13.78	1.97	2.81	0.00	1.81
D_0					
S_0-S_1 Transition Energies Including ZPE Corrections/cm^{-1}					
Experiment[d]	32864	+1891	+1891	+405	+1064
CASSCF[e]	38385	40682	40233	45677	35372
SACCI[f]	33185				
Adiabatic Ionization Energies Including ZPE Corrections/cm^{-1}					
CASSCF (S_1-D_0)	15621	13094	13806		
CASSCF (S_0-D_0)[g]	54006	53777	54039	53620	52390

[a] The wave function consisted of a (14/13,11) active space and was optimized with no state averaging. [b] The wave function consisted of a (10,9) active space; for the S_1 state it was optimized with S_0/S_1 1:1 state averaging. [c] Data from ref 30; the ZPE correction contained in the values was calculated at the MP2/6-31G** level of theory. [d] Values and assignment from ref 15. [e] For the enol tautomers the values were obtained from the wave function described in a, for the keto tautomers from the wave function described in b. [f] Contains no ZPE correction. [g] Values from (14,11)/(13,11)-CASSCF/cc-pVDZ geometry optimizations and frequencies.

frequencies in the translational degrees of freedom, which were, however, within the acceptable limit of 80 cm^{-1} [11] indicating that the potential energy surfaces of CASSCF and SACCI are to a first approximation very similar to each other and of high enough quality to justify the use of CASSCF normal modes and frequencies for the Franck–Condon simulations with SACCI equilibrium geometries.

Suites and Machines. All CASSCF calculations have been performed using the multireference routines implemented in MOLPRO version 2002.6.[23] CIS and SACCI calculations have been carried out with the GAUSSIAN 03[24] ab initio suite. The machines employed were an IBM RS/6000 (4x Power3 375 MHz 64 bit RISC processors, model 44P270, AIX 5.1L, 4 Gb RAM, 64 Gb scratch) and a Linux PC (AMD 64 bit, Ubuntu 5.0, 2.2 Gb RAM, 160 Gb scratch).

3. CASSCF Energies and Geometries

S_0 State. For all tautomers, CASSCF predicts planar geometries with an sp^3 pyramidalized NH_2 group, in line with several MP2 and coupled cluster studies in the literature.[25,26] While for the enol tautomers, the two amino hydrogen dihedral angles have similar values, for the keto tautomers they are significantly nonequivalent, which is almost certainly due to the electrostatic repulsion between the hydrogen attached to the N_1 nitrogen and the amino group hydrogen closest to it. The relative energies of the tautomers obtained from the (14,11)-CASSCF wave function are listed in Table 1. Similar to the coupled cluster values in ref 30, the enol tautomers are higher in energy than the keto tautomers, with the enol N7H as the most energetic form. However, unlike MP2 or CCSD (where the keto N7H form is the lowest energy tautomer) here the keto N9H tautomer is the lowest energy form of guanine. An equivalent prediction is obtained from the smaller (10,9)-CASSCF wave function. A possible explanation for these different energy orderings could be, that unlike CASSCF, the MP2 and coupled cluster wave functions recover the dispersion forces involved in the favorable interaction between the keto group and the hydrogen attached to the N_7 nitrogen thus making the keto N7H tautomer more stable than the N9H tautomer where this interaction cannot occur.

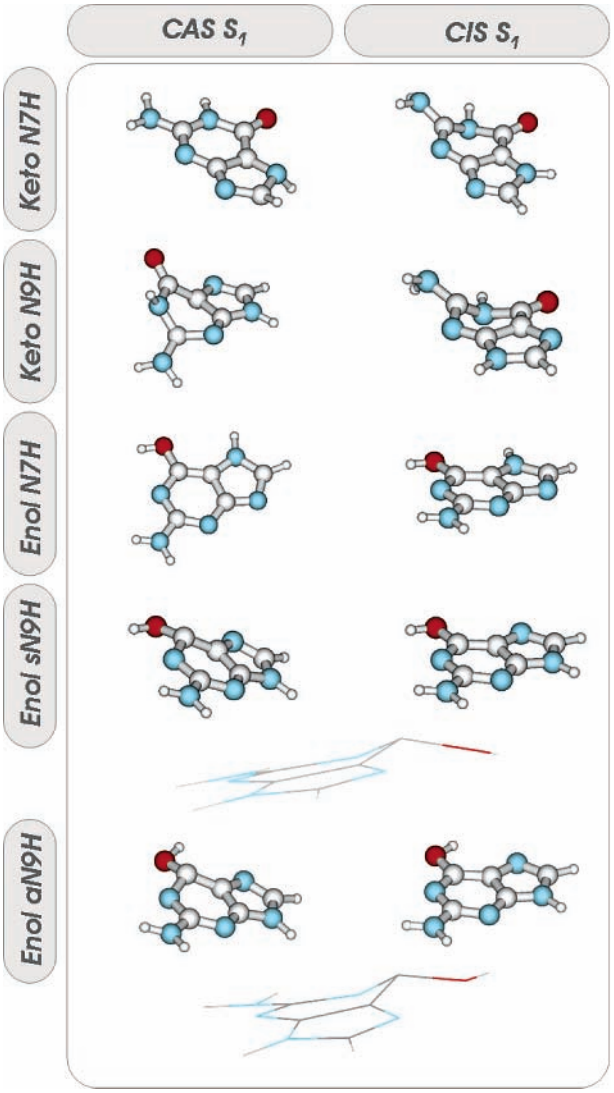

Figure 3. S_1 Equilibrium geometries of the four guanine tautomers and the two rotamers predicted by the CIS/cc-pVDZ and CASSCF/cc-pVDZ level of theory. The CASSCF S_1 state geometry of the enol N9H rotamers is shown from a different perspective highlighting that the distortion predicted by CASSCF affects the aromatic ring system.

S_1 State. The S_1 equilibrium geometries obtained from CIS and CASSCF wave functions are shown in Figure 3. When the two sets of structures are compared an interesting picture arises. As can be seen, the CIS calculations predict that the enol tautomers are fully planar, while the keto forms have largely distorted, nonplanar geometries. Furthermore the S_0-S_1 induced geometry changes are unaffected by the N7H/N9H tautomerism, which is most evident for the keto forms, where both the N9H and N7H tautomers have similar distorted nonplanar geometries. This result is in line with several previous CIS studies, extensively reviewed in ref 27.

The picture looks different for CASSCF. In all cases, the obtained S_1 geometries are nonplanar except for the N7H enol tautomer. This result finds some support in the spectral assignment of the guanine R2PI spectrum suggested by Mons et al. that the first tautomer seen in the spectrum is the enol N7H form, as the small S_0-S_1 geometry change predicted by CASSCF for this tautomer would explain the much more intense $S_1 0^0$ A band origin compared to those of B, C, and D (see Figure S1 in the Supporting Information). Furthermore unlike in CIS, in the CASSCF description the N7H/N9H tautomerism has a marked effect on the equilibrium geometries. Specifically, the N7H tautomers for both the enol and keto forms show smaller nonplanar distortions (in the case of enol N7H none at all) than the N9H tautomers. This result is in line with a study recently conducted by Langer and Doltsinis,[18] who, albeit employing the ROKS method, also observed nonplanar distortions much less pronounced in the keto N7H than the keto N9H form. The puckering angle of the six-membered ring ($C_6N_1C_2N_3$; see Table 2 for atom labeling) calculated in that study is below 10° compared to the 32.2°of the keto N9H tautomer. Our CASSCF predictions are within differences expected to arise between different methodologies not dissimilar to the results obtained by Langer et al. For the same dihedral angle the six-membered ring of the keto N7H form is puckered by about 1° (and being so small cannot be seen in Figure 3), while the puckering of the keto N9H tautomer is much larger reaching 60°. This largely distorted structure has also been found in a recent CASSCF study by Chen and Li[28] on the excited-state deactivation pathways of the guanine keto N9H tautomer, who with a larger (16,12)-CASSCF/6-31G* wave function obtained a value of 117.3° for the $C_4N_1N_3C_2$ dihedral angle, which compares very well with the value of 121.0° of this study.

To understand the effects of the N7H/N9H substitution on the electronic structure of guanine, electron density difference maps between the N7H and N9H enol tautomers obtained from CIS and CASSCF electron densities of the same state have been obtained and are shown in Figure 4a. In both cases the regions with negative electron density difference propagate like linear waves from the N_9 center across the aromatic system losing in size and intensity as they get further away from it. These regions are mirrored in size and shape by positive electron density difference regions propagating from the N_7 center. The similarity between the CIS and CASSCF electron density difference maps does not give an immediate explanation to the substantially different S_1 equilibrium geometries predicted by CIS and CASSCF for the N9H enol tautomer and thus suggests that in the CASSCF picture the 7/9 substitution must affect the electron density redistribution during the S_0-S_1 transition. To demonstrate this point, CASSCF S_0-S_1 electron density difference maps for the 7- and 9-tautomer were obtained and are shown in Figure 4b. Clearly, the two maps are very different. For the 7-tautomer the only large negative difference region is localized underneath the N_{C2} center, rationalizing the S_0-S_1 induced flattening of the amine substituent, as the lone pair orbital acquires more π character donating electron density into the aromatic ring. In the case of the 9-tautomer, the CASSCF S_0-S_1 electron density difference maps show large negative regions and a thus large excitation induced increase in the electron density around the N_1-C_6, C_6-C_5, and C_6-O bonds, which causes a pyramidalisation of the C_6 center and an out-of-plane distorted S_1 equilibrium geometry.

The S_1 relative energy ordering (Table 1) is somewhat different to that of the S_0 state. For the (14,11) active space (only employed with the enol tautomers) the N7H form is the least energetic among the enol tautomers. This is in line with the predicted nonplanar geometry of the latter. Similarly, for the smaller (10,9) active space, the relative stability of the N7H and N9H tautomers is reversed compared to that of the neutral ground state. The relative stability of the keto tautomers, on the other hand, remains unchanged between S_0 and S_1, except that the keto N7H tautomer becomes the most energetic form of guanine (in S_0 it is the enol N7H tautomer). This is reflected in the adiabatic S_0-S_1 transition energies (listed in Table 1)

TABLE 2: S_1-S_0 Induced Geometry Changes of the Enol N7H Tautomer Predicted by HF/CIS, CASSCF, and SACCI/cc-pVDZ Level of Theory

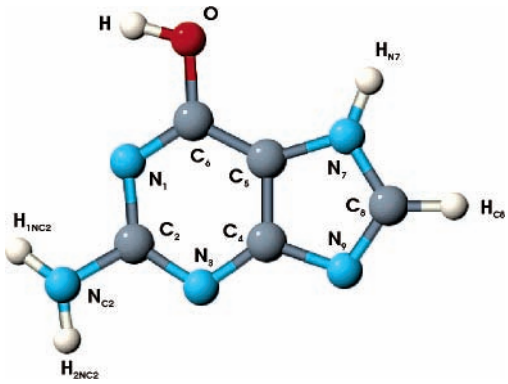

	HF/CIS	CASSCF	SACCI
Bond	S_1-S_0 Bond Length Change/pm		
$O-H$	−0.1	−0.1	−0.2
$O-C_6$	0.9	1.0	1.0
C_6-N_1	3.1	5.7	4.3
N_1-C_2	0.3	−1.2	−1.5
C_2-N_{C2}	−3.5	−3.8	−3.2
C_2-N_3	3.4	5.3	3.9
N_3-C_4	−0.4	0.3	−0.4
C_4-C_5	6.5	5.4	5.4
C_5-C_6	1.0	−0.3	0.3
C_5-N_7	−4.3	−1.2	−2.3
N_7-C_8	7.5	3.9	6.8
C_8-N_9	0.0	1.8	0.5
N_9-C_4	−2.4	−2.5	−2.4
$N_{C2}-H_{1NC2}$	−0.2	−0.2	0.1
$N_{C2}-H_{2NC2}$	−0.2	−0.2	0.2
C_8-H_{C8}	−0.5	−0.4	−0.4
N_7-H_{N7}	0.1	−0.1	−0.1
Angle	S_1-S_0 Angle Change/deg		
$H-O-C_6$	−0.2	−0.3	−0.5
$O-C_6-N_1$	−0.1	−1.5	−1.1
$C_6-N_1-C_2$	−2.0	−2.8	−2.5
$N_1-C_2-N_3$	2.9	3.5	3.4
$N_{C2}-C_2-N_3$	−2.6	−4.2	−3.6
$C_2-N_3-C_4$	0.0	−0.9	−0.5
$N_3-C_4-C_5$	−2.4	−1.9	−2.0
$C_4-C_5-C_6$	1.5	2.0	1.4
$C_5-C_6-N_1$	0.0	0.0	0.2
$C_4-C_5-N_7$	−0.8	−1.9	−1.1
$C_5-N_7-C_8$	1.7	1.8	1.3
$N_7-C_8-N_9$	−3.0	−2.1	−2.6
$C_8-N_9-C_4$	2.2	1.2	1.8
$N_9-C_4-C_5$	0.0	1.0	0.8
$H_{1NC2}-N_{C2}-H_{2NC2}$	5.4	7.3	4.5
$H_{1NC2}-N_{C2}-C_2$	4.1	5.9	2.6
$H_{C8}-C_8-N_9$	2.8	1.2	2.3
$H_{N7}-N_7-C_8$	−0.3	−0.7	−0.4
Dihedral	S_1-S_0 Dihedral Change/deg		
$H-O-C_6-N_1$	−0.6	−0.4	0.2
$H_{1NC2}-N_{C2}-C_2-N_1$	−22.9	−28.5	−11.6
$H_{1NC2}-N_{C2}-C_2-N_3$	−19.5	−22.0	−8.2
$N_{C2}-C_2-N_1-N_3$	1.5	2.7	0.7
$H_{N7}-N_7-C_5-C_8$	0.4	0.2	−0.1

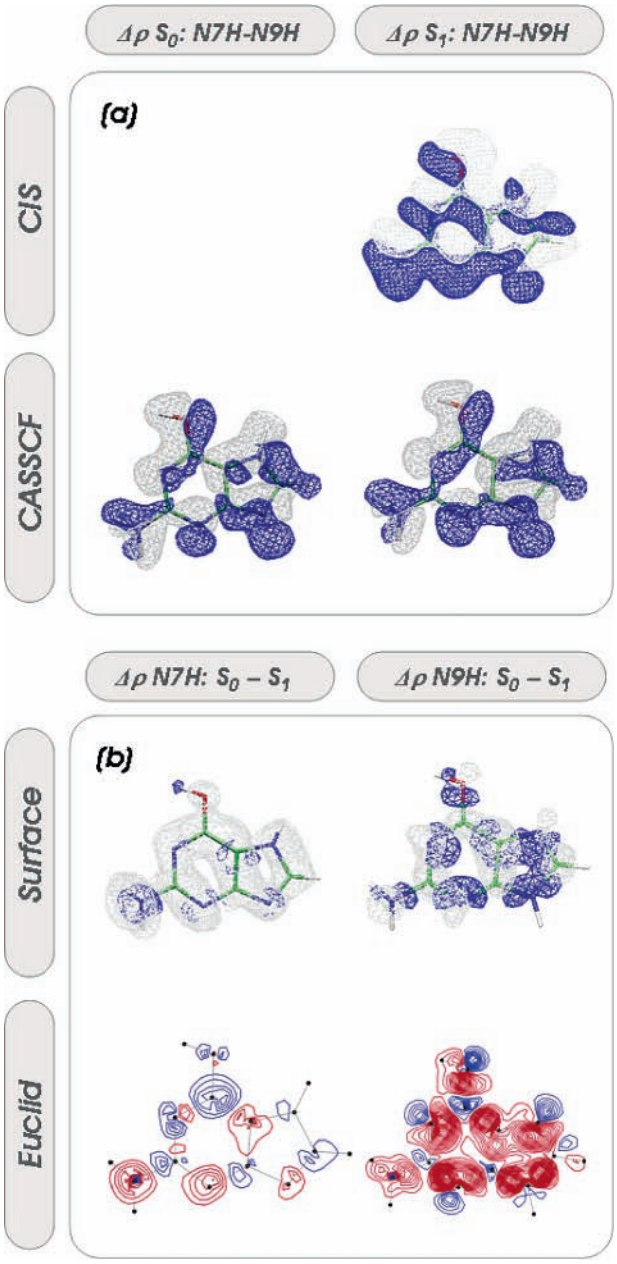

Figure 4. (a) Electron density difference plots between the guanine enol N7H and enol sN9H tautomers illustrating the effects of the N7H−N9H substitution. In the case of CIS, the differences were obtained by subtraction electron densities of single-point calculations on the CIS S_1 ($\Delta\rho$ S_1: N7H−N9H) equilibrium geometries. In the case of CASSCF, single-point calculations were carried out on the CASSCF S_0 equilibrium geometry for both the S_0 and S_1 states giving rise to the $\Delta\rho$ S_0: N7H−N9H and $\Delta\rho$ S_1: N7H−N9H electron density difference plots, respectively. (b) Electron density difference surface and contour (Euclid) plots between the S_0 and S_1 CASSCF wave functions obtained from single-point calculations on the CASSCF S_0 equilibrium geometries of the enol N7H and enol sN9H tautomers, respectively. For the surface plots, gray regions indicate positive, blue regions negative density difference values, while for the contour plots the blue contours are positive and the red contours negative density differences.

where the keto N7H tautomer has the largest S_0-S_1 ΔE. The keto N9H tautomer being the most energetically stable in both states has the smallest transition energy. As already mentioned in the Introduction, substitution studies have demonstrated that the lowest and highest energy band origin (bands A and D) are due to enol tautomers, while the keto tautomers give rise to the energetically intermediate bands B and C. Clearly, the large discrepancy between theory and experiment indicates that the CASSCF methodology is inadequate for accurately describing the S_1 potential energy surface of the keto tautomers. For the enol tautomers, however, the predictions are of better quality. Although their calculated transition energies are overestimated by approximately 6000 cm^{-1} compared to those from experiment (assuming the assignment by Mons et al. is correct), the relative difference between the two transition energies of 2297 cm^{-1} is very similar to the experimental value of 1891 cm^{-1}. This result further supports the prediction made by CASSCF that the N9H S_1 geometry is distorted, whereas that of the N7H tautomer is planar. It furthermore indicates that unlike for the keto tautomers, here CASSCF delivers a good description of the S_1 potential energy surface.

Effects of the Rotamerism in the Enol N9H Tautomer. Unlike enol N7H (where it is energetically unfeasible), in the enol N9H tautomer the OH group can be orientated facing away or toward the five-membered ring, giving rise to two rotamers, called syn and anti, respectively (in all relevant tables and figures referred to as enol-aN9H and enol-sN9H). While the preceding analyses focused solely on the syn rotamer, here we would like to give a short account on the effects of the rotamerism in the enol N9H tautomer. This is of particular interest, as in a recent paper Chin et al.[29] tentatively reassigned band D to the anti rotamer. The CASSCF calculations carried out here predict the energetics between the two rotamers to be very similar. As can be seen in Table 1, the relative energies in the ground state differ by 3.76 kJ/mol with the syn rotamer being lower in energy than the anti, most probably due to the favorable interaction between the OH hydrogen and the lone pair on the N_1 center arising when in syn configuration. In the S_1 state the difference is smaller (1.63 kJ/mol), but the energy ordering is reversed compared to that of the ground state. The largest difference of 6.90 kJ/mol occurs in the cationic ground state, and the energy ordering follows that of the neutral ground state. The S_1 state optimized (14,11)-CASSCF/cc-pVDZ geometry of the anti rotamer is similar to that of the syn rotamer, with a comparable out-of-plane distortion of the C−O bond (see Figure 3), and a reasoning similar to that discussed in the last section of the preceding paragraph for the syn rotamer applies to this finding. The S_0-S_1 transition energy is 450 cm^{-1} lower compared to that of the syn rotamer. This brings the transition energy difference between the N7H and aN9H tautomers down to 1847 cm^{-1}, which is much closer to the experimental difference of 1891 cm^{-1} than that predicted between the N7H and sN9H tautomers of 2297 cm^{-1}, thus giving considerable support to the assignment of band D to the anti rotamer as suggested in ref 29.

D_0 State. For all tautomers, CASSCF predicts fully planar geometries. Unlike the neutral ground state, here the NH_2 group is sp^2 hybridized and the amino hydrogens are in plane with the aromatic ring system. Similarly to the S_0 state, a comparable energy ordering is obtained with the enol N7H tautomer as the highest and the keto N9H tautomer as the lowest energy form of cationic guanine, although the energy differences between the isomers have increased.

4. Vibronic Simulations with CASSCF Geometries

To gain a qualitative view regarding tautomer assignment, Franck−Condon simulations of the tautomer-specific R2PI spectra were generated from CASSCF equilibrium geometries and are shown in Figure 5. For comparison the experimental R2PI spectra recorded by Nir et al. and Mons et al. with labeled origin bands (A−D) and the vibronic simulations with HF/CIS equilibrium geometries can be found in Supporting Information

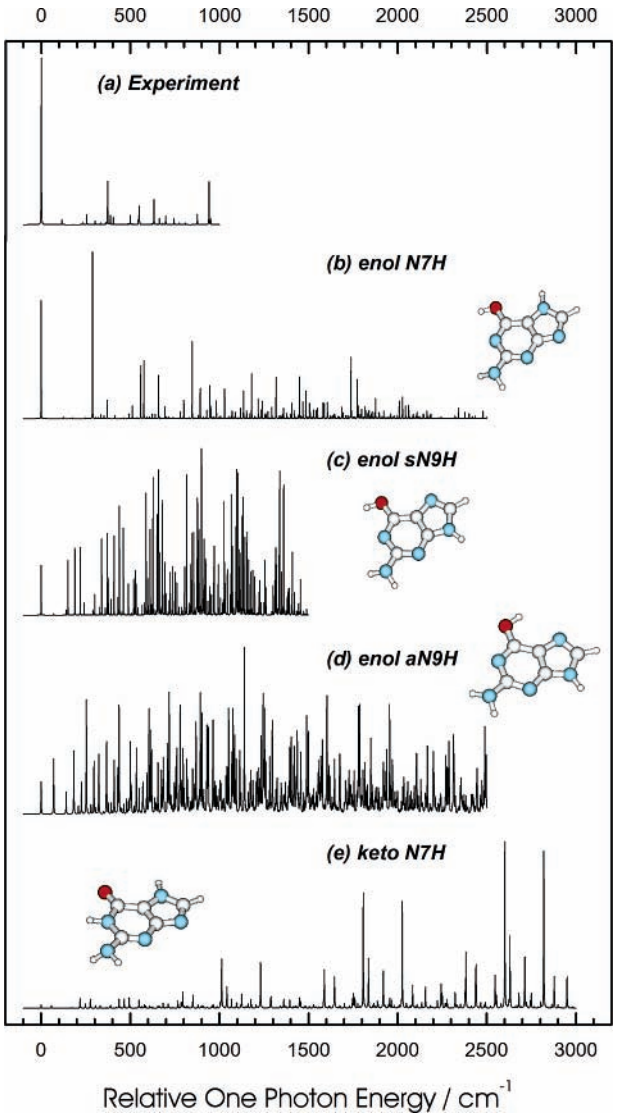

Figure 5. Tautomer-specific Franck−Condon simulations of the R2PI spectrum of guanine obtained from the S_0 and S_1 equilibrium geometries and normal modes calculated at the (11,14)-CASSCF/cc-pVDZ and (10,9)-CASSCF/cc-pVDZ levels of theory for the enol and keto tautomers, respectively; (a) shows the experimental R2PI spectrum which was reproduced by fitting Lorentzian line shapes to intensities taken from ref 13.

Figures S1 and S2, respectively. The simulations are compared and analyzed in terms of their qualitative similarity to experiment and relative origin transition intensities. The authors are aware of the fact, extensively discussed in ref 15, that the intensity of the origin transitions of the different tautomers is strongly dependent on the setup and type of desorption source used, and therefore, comparisons between calculated and experimental transition intensities are made with this issue in mind. In the R2PI spectra of Nir et al.[13] and Mons et al.[15], the intensity ratios A/B/C/D of the origin bands are 17:2:1.3:1 and 6:1:1.3:5.7, respectively. Thus, the major differences of the latter to the former spectrum are the origin transitions of the keto tautomers (bands B and C), being more intense and furthermore band D, being almost as intense as band A.

Enol Tautomers. A comparison between the Franck−Condon simulations of the N7H and the syn and anti N9H enol tautomers obtained from HF/CIS and CASSCF equilibrium geometries show some characteristic differences. For the N7H tautomer, the first intense transitions occur 250 cm^{-1} above the origin transition, while for the two rotamers of the N9H tautomer intense transitions result as early as 50 cm^{-1} above the origin. The large gap observed in the simulations of the N7H tautomer qualitatively mirrors the experimental spectrum. Furthermore, due to similar S_0-S_1 geometry changes predicted by both the CIS and CASSCF wave functions, the rotamerism in the enol N9H tautomer has only very small effects on the appearance of the Franck−Condon simulations, and in the following discussion reference to the enol N9H tautomer includes both rotamers unless otherwise specified.

Accounting for the difference in the magnitude of the transition dipole moments of the two tautomers ($||\mu_{N7H}||/||\mu_{N9H}|| = 0.82$), the intensity of the origin transition obtained from simulations with HF/CIS equilibrium geometries of the N7H and N9H tautomers are fairly similar, with an approximate ratio of 8:1. This is a direct result of the similarity in the geometry changes predicted at the CIS level of theory: the flattening of the NH_2 group upon excitation brings the geometry from pseudo-C_s to C_s symmetry. The intensity ratio is comparable to the ratio between band A and band D in the experimental spectrum of Mons et al.[15] and supports their assignment of band A to the N7H tautomer and band D to the N9H tautomer.

The origin transition intensity of the N7H and N9H enol tautomers obtained from the simulations of the CASSCF equilibrium geometries show a much larger difference, compared to that of HF/CIS. Accounting for the magnitude of the transition dipole moments of the two conformers ($||\mu_{N7H}||/||\mu_{N9H}|| = 0.85$) the much higher intensity ratio of 50:1 is obtained which is due to the much larger S_0-S_1 induced geometry change of the N9H tautomer. This intensity ratio is not reflected in the experimental ratios of the enol tautomers (bands A and D) found by Mons et al., but it is comparable to the experiment by Nir et al. thus lending some support to the nonplanar S_1 state geometry.

Keto Tautomers. Near-zero origin transition intensities are observed in the simulated spectra obtained from the CIS geometries of both keto tautomers and the CASSCF geometries of the keto N9H tautomer, and thus their Franck−Condon simulations are not presented. The large geometry changes induced by the electronic excitation predicted by both the CIS and CASSCF wave functions make the overlap integrals zero. The vibronic intensities obtained from the keto N7H CASSCF geometries are larger than for the simulations of the keto N9H tautomer but much smaller compared to those of the enol tautomers. The moderate S_0-S_1 geometry change predicted by CASSCF causes the overlap with the higher energy normal-mode vibrational wave functions to increase making the vibronic transition intensities associated with these modes much stronger compared to the vibrationless origin. This gives the simulated spectrum the characteristic parabolic shape of an extended Franck−Condon envelope (see Figure 5d).

Although the simulated low/near-zero origin transition intensities agree with the assignment of band B and C to the two keto tautomers given by Mons et al.[15] and Nir et al.,[13] in all simulations the ratio between the origin transition intensities of the keto tautomers (bands B and C) and those of the enol tautomers is considerably smaller than found experimentally. One reason for this discrepancy can be attributed to the fact that the experimental transition intensities are not only affected by Franck−Condon overlaps and transition dipole moments but also by the relative abundance of the tautomers in the molecular beam, a parameter not included in this analysis. An abundance in the molecular beam that is larger for the keto than the enol tautomers is supported by the study of Hanus et al.,[30] who found the keto forms to be energetically considerably more stable at the RI-MP2/TZVPP, MP2/aug-cc-pVDZ and CCSD(T)/aug-cc-

TABLE 3: Summary of Rotational Constants and Transition Dipole Moments (TDM) for the Enol N7H Tautomer

	rotational constants		
	A	B	C
HF/CIS/cc-pVDZ			
S_0	1947.77	1148.84	722.97
S_1	1885.93	1157.07	717.11
|TDM|	0.6722	1.2142	0.0001
CASSCF/cc-pVDZ			
S_0	1927.80	1139.49	716.65
S_1	1864.90	1141.54	708.10
|TDM|	0.2331	0.9532	0.0001
SACCI/cc-pVDZ			
S_0	1927.28	1136.81	715.45
S_1	1870.94	1143.15	709.85
S_1 displaced	1865.86	1140.45	708.12
|TDM|	0.5428	1.1533	0.0007

pVDZ levels of theory. Owing to their large stability, the keto tautomers are probably so abundant as to compensate for their very small Franck−Condon overlaps and thus can still be observed in the spectrum. The much less stable and thus less abundant enol tautomers, however, with their much larger Franck−Condon factors and oscillator strengths[31] give rise to much more intense vibronic transitions (at least in the case of band A, the enol N7H tautomer).

5. Vibronic Simulations with SACCI Geometries

The small S_0-S_1 geometry changes predicted by CASSCF for the enol N7H tautomer and the closer qualitative resemblance of its simulated spectrum to experiment (compared to the simulated spectra of the syn and anti enol N9H tautomers) strongly suggest it to be the most likely candidate giving rise to the origin band A and associated vibronic features of the guanine R2PI spectrum. An enlarged view of the simulation in the first 700 cm^{-1} (see Figure S5 in the Supporting Information) however shows that the CASSCF equilibrium structures fail to reproduce the experimental vibronic intensities faithfully. Taking on board the results from studies 11 and 12, SACCI geometry optimizations have been carried out to obtain more refined structures. As in the case of phenol and phenol−nitrogen,[11,12] the SACCI wave functions bring only slight alterations to the CASSCF equilibrium structures, but despite these small predicted differences, significant changes in the simulated vibronic transition intensities can be observed. This is because Franck−Condon factors are sensitive to changes down to the picometer region.

S_0-S_1 Geometry Changes. The calculated S_0-S_1 induced changes for the N7H enol tautomer are shown in Table 2. All ab initio methods employed predict large changes in the bonds forming the aromatic system: C_4-C_5, C_6-N_1, C_2-N_3, and N_7-C_8 lengthen, while large contractions occur in bonds C_5-N_7 and N_9-C_4, causing the aromatic system on the whole to expand. This is reflected in the change of the rotational constants listed in Table 3, where an average decrease of 60 MHz in the A constant can be observed. Constant B increases by about 6 MHz indicating that in the overall expansion of the aromatic system a small contraction occurs along the short *b*-axis. The S_0-S_1 induced ring expansion is comparable to that observed by Callis et al.[19] for the S_0-S_1 (^1L_b) transition of indole. The calculated transition dipole moments for the guanine enol N7H tautomer (listed in Table 3) clearly indicate that also here the $S_1(\pi\pi^*)$ state is an L_b state, with the transition dipole moment angle being 61° for CIS, 76° for CASSCF, and 65° for SACCI with respect to the long *a*-axis. This angle is very close to the experimentally determined value of 62.2° in indazole for the $S_1(^1L_b)-S_0$ transition.[32] The S_0-S_1 transition also affects the geometric parameters of the amine and hydroxyl sustituents. The C_2-N_{C2} bond experiences a large contraction, while the C−O bond, in contrast to phenol and phenol−nitrogen,[11,12] lengthens. More importantly, the effects of the electronic excitation on the dihedral angles of the amine hydrogens are substantial with CASSCF predicting the largest and SACCI the smallest change. In the ground state, the dihedral angles are much smaller compared to those of CIS and CASSCF, while in the S_1 state they are larger, leading to a slightly nonplanar geometry compared to the C_s planar geometry in CIS and CASSCF. Inspection of Table 1 shows that the adiabatic S_0-S_1 transition energy predicted by SACCI of 33185 cm^{-1} is much closer to the experimental value of 32864 cm^{-1} compared to that of CASSCF, suggesting that geometry changes calculated by the coupled cluster wave function are more accurate, and indeed it reflects the substantially higher quality of the SACCI-optimized geometries.

SACCI Simulations. The Franck−Condon simulation of the R2PI spectrum of the enol N7H tautomer obtained from SACCI equilibrium geometries is shown in Figure 6b. An inspection of Table 2 reveals that compared to the SACCI, CIS and CASSCF predict much larger changes in the dihedral angles of the amine hydrogens. Thus, in the simulations obtained from CIS and CASSCF equilibrium geometries, the vibronic transition associated with the NH_2 out-of-plane bend $\beta''(NH_2)$ is more intense than in the simulation with SACCI-optimized geometries. Overall a good resemblance to the experiment is obtained if a scaling of 94% is introduced to the harmonic frequencies (not shown in the figure). The small features at 240, 260, and 300 cm^{-1} can readily be assigned to the first overtones of modes $1\beta''_b(r)$ (mode 1) and $\beta''(H_{N7})$ (mode 2) and the 6-ring gearing mode fundamental 15 (mode 6), respectively. Interestingly, an ambiguity arises as to which mode can be associated with the band at 337 cm^{-1}. The simulation suggests an assignment to the NH_2 in-plane bend (mode 8), as proposed by Nir et al.[13] (only for the N9H tautomer). The NH_2 out-of-plane fundamental (mode 9) is as intense as the NH_2 in-plane bend and could be assigned, together with the OH torsion τ(OH) (mode 10), to the small features in close proximity to the blue of the band at 337 cm^{-1} (355 and 365 cm^{-1}). As can be seen from Figure 7, the latter two modes are actually combinations between the NH_2 out-of-plane bend and the OH torsion, which explains why in the SACCI simulation transitions to the OH torsion are observed (as coupled to the NH_2 out-of-plane), while in the HF/CIS and CASSCF simulations such transitions are not present.

The assignment of the NH_2 out-of-plane bend to the band at 355 cm^{-1} in the experimental spectrum suggests that the geometry change in the dihedral angles of the amine hydrogens is, although smaller than for CIS and CASSCF, still overestimated by SACCI and that in the true S_1 equilibrium structure the hydrogens of the NH_2 group are not in the plane of the aromatic system. This is in line with findings on other aromatic systems with an amine substituent where the amine group flattens with increasing electronic excitation with C_s symmetry only reached in the ground state of the ion.

The band at 475 cm^{-1} in the experimental spectrum approximately coincides with the 6-ring breathing mode 6a (mode 12) fundamental. This is in agreement with the tentative assignment by Nir et al.,[13] although again for the N9H rather than the N7H enol tautomer. The intensity, however, is slightly lower than in the experiment, suggesting that the C−O bond change affecting the intensity of the band associated with this

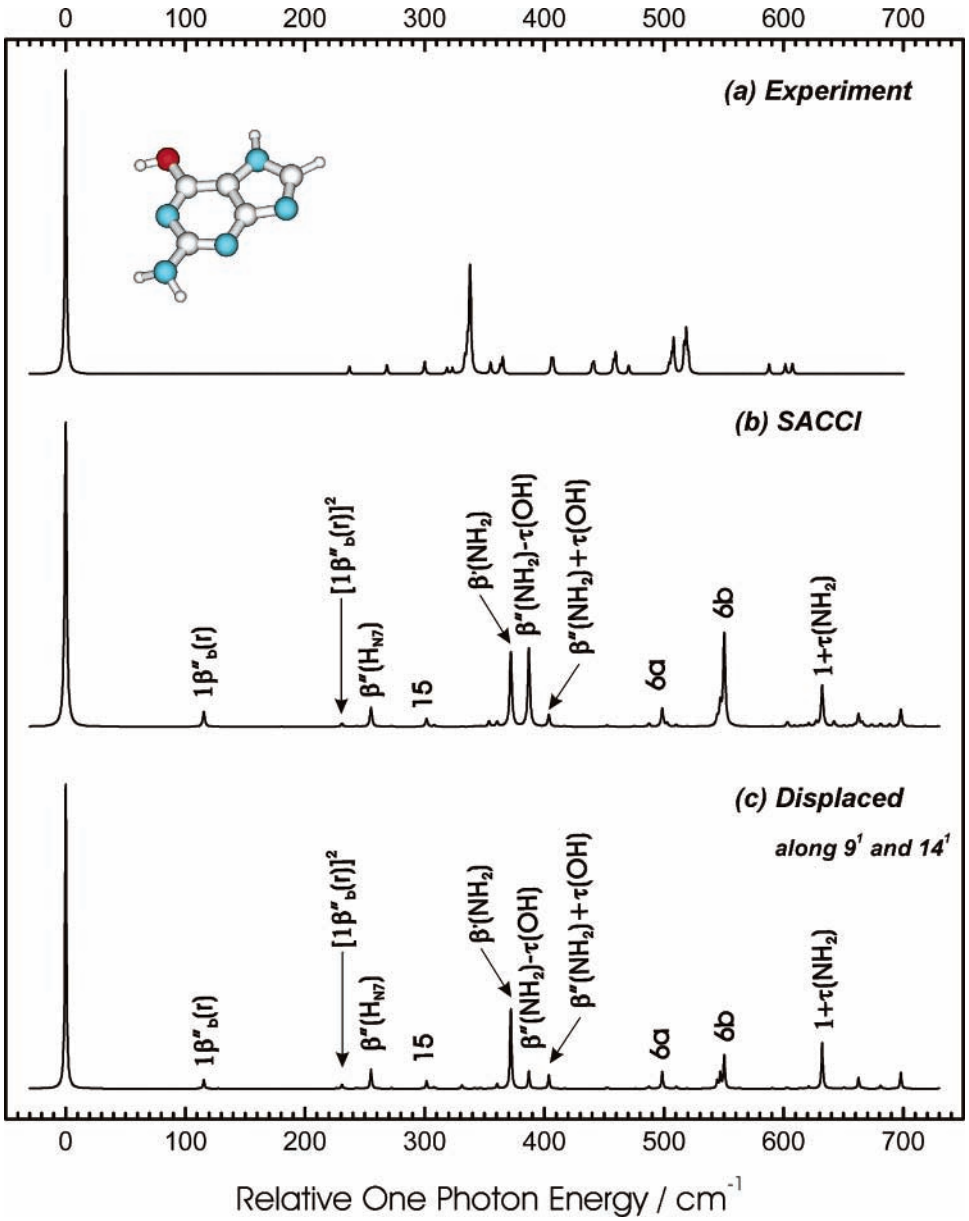

Figure 6. Experimental (a) and simulated R2PI spectra of the enol N7H tautomer using (b) SACCI-optimized and (c) fitted geometries. The intensities are plotted with their associated frequencies and labels listed in Table 4. The experimental R2PI spectrum was reproduced by fitting Lorentzian line shapes to intensities taken from ref 13.

mode (as in the case of phenol and phenol−nitrogen) is underestimated. The bands at 508 or 517 cm^{-1}, with a difference of 50 cm^{-1} could be assigned to 6-ring breathing mode 6b (mode 14). The band labeled in the simulation as mode 6b is in fact composed of three overlapping lines/bands, associated with the first overtone of $2\beta''_b(r)$ (mode 5), $\gamma''_a(r)$ (mode 13), and 6b (mode 14). However, the most prominent among these is mode 6b and the intensity of the band associated with this mode is overestimated.

Simulation with Empirically Corrected Structures. To improve on the shortcomings of the SACCI geometries, Franck−Condon simulations with the S_1 SACCI equilibrium geometry displaced along selected (8,8)-CASSCF normal modes have been carried out until a good agreement to experiment was obtained. As discussed in the previous paragraphs, the SACCI simulation overestimates the intensity of the bands associated with transitions to the NH_2 out-of-plane bend (mode 9) and to the ring breathing mode 6b (mode 14). Thus, the S_1 geometry was modified along the coordinates of these two modes. Displacement along the NH_2 out-of-plane bend coordinate that decreased the change in the NH_2 dihedral angles (−4.9° and −8.8°) lowered the intensity of the band associated with the NH_2 out-of-plane bend, while the displacement along the normal coordinate 6b (mode 14) was carried out such to increase the six-membered ring expansion. As can be seen from the rotational constants in Table 2, only small changes in the S_1 equilibrium structure along modes $\beta''(NH_2)$ and 6b were necessary to obtain a spectrum in very good agreement to experiment (see Figure 6c), indicating that despite its shortcomings the SACCI equilibrium geometry is very accurate and more importantly lending strong support to a band assignment based on the SACCI simulations.

Assignments of the individual experimental bands to normal modes as suggested by the SACCI simulations are listed in Table 5 together with the band assignments by Nir et al.[13] and Piuzzi et al.[14] From this table it is clear that most of the band assignments by Nir et al., although for the enol sN9H tautomer, coincide with those proposed in this study. The very good agreement to experiment of the simulated and fitted spectra obtained from SACCI geometries strongly supports an assign-

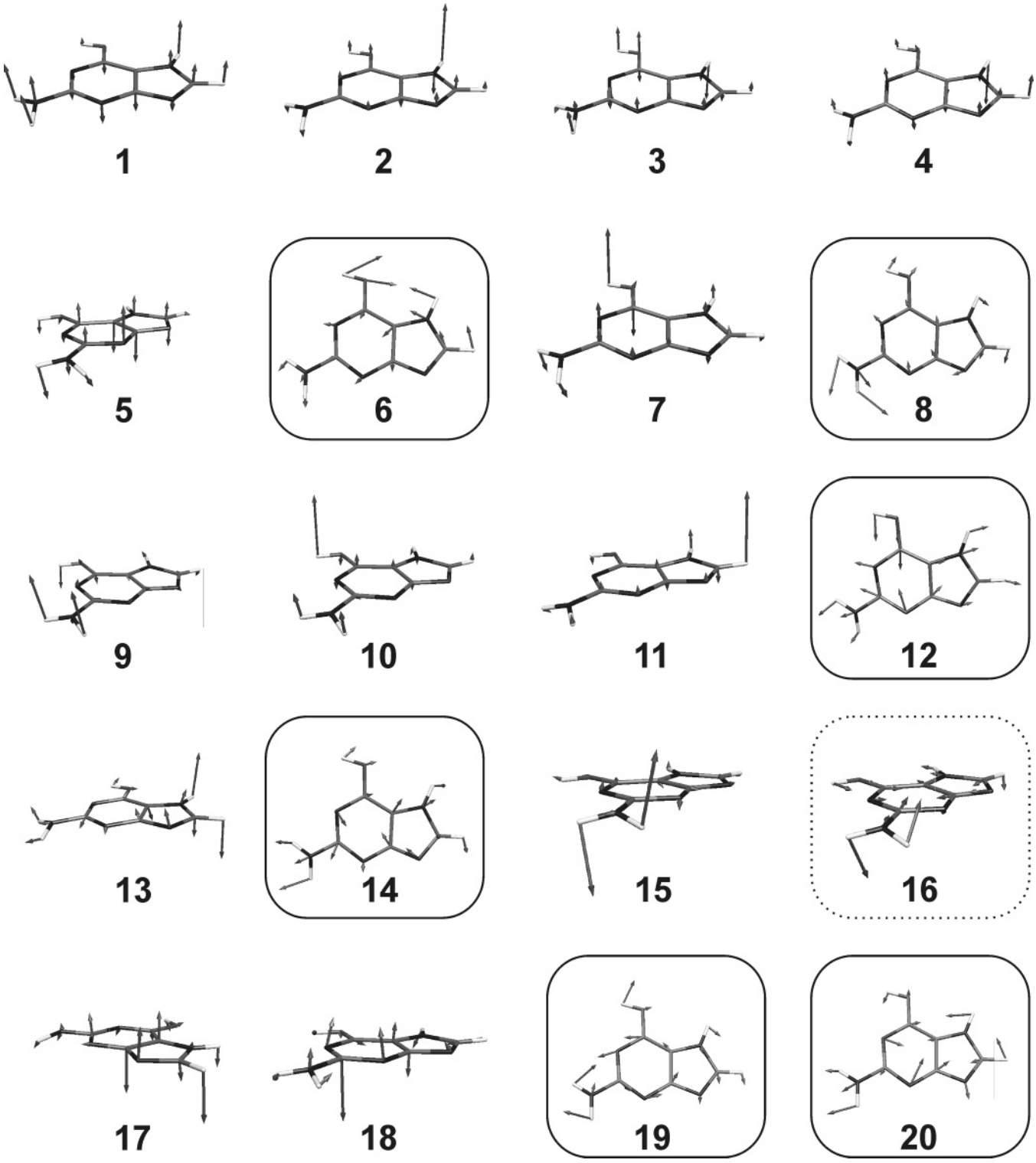

Figure 7. First 20 S_1 normal modes of the (8,8)-CASSCF/cc-pVDZ frequency analysis on the S_1 SACCI/cc-pVDZ equilibrium geometry of the enol N7H tautomer are shown. The vibrations are sorted by increasing frequency; the mode numbers can be related to the mode notation used in the text and figures by means of Table 4. The pseudo in-plane vibrations are boxed. Mode 16 is boxed with a dotted line as it consists of in-plane and out-of-plane displacements.

ment of band A to the enol N7H tautomer. One could say at this point of the discussion that only SACCI calculations on the syn and anti enol N9H tautomer would further strengthen the above assignment. However, owing to the perturbation selection of the excitation operators, the SACCI method can only bring about small changes in the starting geometry, and therefore a SACCI geometry optimization on the N9H tautomers would have not affected the nonplanar S_1 state geometry enough to change the overall characteristics of their spectra (the parabolic shape of the Franck−Condon envelope due to the large S_0-S_1 induced geometry change) in order to undermine the above assignment.

6. Discussion

Enol N7H Tautomer. The vibronic analyses shown and discussed in the previous sections allow for a confident assignment of band A and its associated vibronic features to

TABLE 4: S_1 Frequencies of the Enol N7H Tautomer of Guanine[a]

CASSCF frequency on SACCI geometry				
MN	description	phenol	label	n
1	ring bend around b	10a	$1\beta''_b$ (r)	116
2	H_{N7} bend		$\beta''(H_{N7})$	128
3	6-ring bend around a	10b	$1\beta''_a$ (r)	180
4	5-ring bend around a	16a	$2\beta''_a$ (r)	226
5	ring zigzag mode around b		$2\beta''_b$ (r)	272
6	**6-ring gearing**	**15**	**15**	**302**
7	OH torsion	4	$\tau(OH) - \beta''(NH_2)$	331
8	**NH_2 bend**		**$\beta'(NH_2)$**	**372**
9	NH_2 bend		$\tau(OH) - \beta''(NH_2)$	387
10	$\tau(OH) + NH_2$ bend	$\tau(OH)$	$\tau(OH) + \beta''(NH_2)$	404
11	H_{C8} bend	11	β'' (H_{C8})	473
12	**6-ring breathing**	**6a**	**6a**	**499**
13	5-ring wag	16a	γ''_a (r)	547
14	**6-ring breathing**	**6b**	**6b**	**550**
15	$\tau(NH_2)$		$\tau(NH_2)$	621
16	**phenol like 1 + $\tau(NH_2)$**	**1**	**1 + $\tau(NH_2)$**	**632**
17	5-ring zigzag mode	16b	5z	651
18	6-ring zigzag mode	16b	6z	681
19	**6- and 5-ring gearing**	**3**	**3**	**698**
20	**6-ring breathing**	**18a**	**18a**	**875**

[a] MN = mode number; ν = frequencies in cm^{-1}; τ = torsion; β'' = out-of-plane bend; β' = in-plane bend, γ'' = out-of-plane wag. In-plane vibrations are in bold. Comparable vibrations of phenol are listed. Only the labels for the phenol in-plane vibrations have been used to label corresponding guanine normal modes. In transferring the labels no consideration was given to the fact that in phenol the OH bond is along the *a*-axis, while in guanine it is along the *b*-axis.

the enol N7H tautomer. Its sharp spectral bands and the very good agreement between experiment and the calculated normal modes and simulated spectra indicate that within the energy window analyzed there are no conical intersections with the electronic ground state or vibronic coupling to a possible nπ^* state and the potential energy surface is to a good degree harmonic.

Enol N9H Tautomers. The simulations of the vibronic spectra of the enol N9H tautomers show a significant Franck−Condon activity that is not observed experimentally. Population labeling IR−R2PI spectra of the band assigned to the anti enol N9H tautomer by Chin and co-workers (band D) show no Franck−Condon envelope.[29,33] Due to the absence of sharp features in the dispersed fluorescence (DF) spectrum of species D, otherwise present in the DF spectra obtained from bands A, B, and C, it was proposed that a strong coupling between the $\pi\pi^*$ and nπ^* potential energy surfaces exists that results in a conical intersection below the first quantum of the lowest energy normal mode causing a nonradiative decay onset that effectively quenches transitions to any normal mode but the vibrationless origin. This coupling makes the potential energy surface strongly anharmonic, and therefore the absence of the Franck−Condon envelope is not reproduced in the simulations of the enol N9H tautomers as they are based on the harmonic approximation. The nonplanar S_1 geometry predicted by the CASSCF wave function lends support to the photochemistry proposed by Chin and co-workers especially because the main out-of-plane distortion occurs on the aromatic ring system (see Figure 3). As this is the case for both rotamers, it furthermore suggests that in the CASSCF description the rotamerism has probably little effect on the photochemistry of the enol N9H tautomer.

Keto N9H Tautomer. Both CIS and CASSCF predict strong puckering of the six-membered purine ring around the position of the amine group substituent. The geometry obtained is comparable to the $S_0/S_1(\pi-\pi^*)$ conical intersection (CI) structures of 2-aminopurine,[20] adenine,[34] and the $S_0/S_1(\pi-n_N\pi^*)$ conical intersection geometry of the cytosine keto tautomer[22] (albeit the puckering is more pronounced). The similarity between the guanine keto N9H S_1 equilibrium structure and the S_0/S_1 CI of molecules analogous to guanine suggests that the energy difference between the two structures is small and that a transition state barrier, if it even exists, is very low in energy. This sets the conditions for efficient internal conversion to the ground state and thus could explain the subpicosecond S_1 state lifetime of guanine observed experimentally in ref 35. Furthermore, it suggests that the S_1 potential energy surface is very anharmonic, and Franck−Condon algorithms based on the harmonic approximation are inadequate for vibronic simulations of the keto N9H tautomer. A recent CASSCF/CASPT2 study by Chen and Li[28] on the nonradiative decay mechanisms of the electronically excited keto N9H tautomer lends some support to the above hypothesis, as they observed a small activation barrier of 1.7 kcal/mol required for the system to get from the S_1 $\pi-\pi^*$ minimum to the $S_0/S_1(\pi-\pi^*)$ CI.

Keto N7H Tautomer. The S_1 state geometry of the keto N7H tautomer is substantially different to that of the keto N9H tautomer, and it is also quite dissimilar to the CI structures of the guanine analogues 2-aminopurine and adenine. No puckering of the six-membered purine ring around the position of the amine group substituent occurs; instead the hydrogens on the five-membered ring are located above and below the plane of the aromatic ring system. Provided that a conical intersection to the ground state has an equilibrium structure similar to that of 2-aminopurine or adenine, it is reasonable to suggest that the transition state barrier between the S_1 equilibrium and the possible CI structure is larger in energy than for the keto N9H tautomer.

7. Concluding Remarks and Outlook

The IR−UV deconvolution of the guanine and recently also the guanine−water R2PI spectra[36] has not been able to unambiguously answer the question whether the first species observed in the spectra is the N7H or N9H enol tautomer. The CASSCF calculations presented in this study suggest that the 7/9 substitution has a drastic effect on the electronic structure of the S_1 state, leading to substantially different simulated spectra and providing strong evidence that the first tautomer seen in the guanine R2PI spectrum is the enol N7H form. On the basis of this fact it is reasonable to suggest that also in the guanine−water spectrum the first species is most probably the enol N7H structure as in recently recorded R2PI spectra of phenylalanine−water clusters it was observed that the water molecule does not affect the monomer structures and their relative abundance in the molecular beam but rather finds a way to bind to them.[37] We furthermore envisage that Franck−Condon simulations on guanine−water clusters using SACCI geometries with CASSCF frequencies will represent a substantial aid in resolving the enol N7H versus N9H quandary and perhaps also deliver decisive information in a similar dilemma affecting the assignment of the R2PI spectrum of the guanine−cytosine base pair.[4,8]

Ultimately, the enol N7H/N9H quandary can be resolved with future zero electron kinetic energy (ZEKE) or the mass-resolved counterpart mass analyzed threshold ionization (MATI) studies. Not only will a precise determination of the ionization potentials be of help, but unlike R2PI, through a two-color excitation/ionization scheme, tautomer-specific ZEKE/MATI spectra can be obtained facilitating assignment. Furthermore, if the predictions about the S_1 state geometries of the enol N7H and N9H tautomers made by CASSCF are right, then a parabolic shaped Franck−Condon envelope can be expected for the latter

TABLE 5: Peak Assignment for the Guanine R2PI Spectrum (Energy Window 0−650 cm^{-1}) by Nir et al. and Assignment Based on the Franck−Condon Simulations Obtained from the Enol N7H S_0 and S_1 SACCI Equilibrium Geometries with Their respective (8,8)-CASSCF Frequencies[a]

		assignment by Nir et al.[b]		our assignment	
peak no.	exptl	description	CIS MN	description	SACCI
0	0	origin tautomer A			
1	237	n−π* transition of A[c]		1β''_b (r)	$\mathbf{1^2}$ (232)
2	268	n−π* transition of A[c]		$\beta''(H_{N7})$	$\mathbf{2^2}$ (256)
3	300	n−π* transition of A[c]		15	$\mathbf{6^1}$ (302)
4	319	n−π* transition of A[c]		$\beta''(H_{N7})$, 2β''_a (r)	$\mathbf{2^1 4^1}$ (354)
5	323	n−π* transition of A[c]		1β''_a (r)	$\mathbf{3^2}$ (361)
6	338	inp ring gearing + C−N bending	34 (365)	$\beta'(NH_2)$	$\mathbf{8^1}$ (372)
7	355			τ(OH) − $\beta''(NH_2)$	$\mathbf{9^1}$ (387)
8	365			τ(OH) + $\beta''(NH_2)$	$\mathbf{10^1}$ (404)
9	406	origin tautomer B			
10	441	tautomer B[c]			
11	457	6-ring stretch (phenol 6a)	33 (492)	6a	$\mathbf{12^1}$ (499)
12	471	tautomer B[c]			
13	508	inp zigzag mode of the 2 rings	31 (554)	γ''_a (r)	$\mathbf{13^1}$ (547)
14	517			6b	$\mathbf{14^1}$ (550)
15	588			2β''_b (r), τ(OH)	$\mathbf{5^1 7^1}$ (604)
16	601			$\tau(NH_2)$	$\mathbf{15^1}$ (621)
17	607	ring breathing mode 1	28 (653)	1 + $\tau(NH_2)$	$\mathbf{16^1}$ (632)

[a] MN = mode number; the figures in brackets are the energy in cm^{-1} of the respective mode. [b] Assignment from ref 13. [c] Assignment from ref 14.

tautomer in both the syn and the anti rotamer configuration. For future reference, vibronic simulations of the ZEKE/MATI spectra obtained from geometries and normal modes at the CASSCF/cc-pVDZ level of theory have been carried out and can be found in the Supporting Information, Figure S6.

In line with the studies of phenol and phenol−nitrogen in refs 11 and 12, refining the enol N7H tautomer CASSCF-optimized geometries with SACCI and determining CASSCF normal modes at these SACCI structures has proven to be a successful strategy for generating simulations in good agreement with experimental spectra. There are still shortcomings, suggesting that SACCI calculations with larger excitation spaces are required to generate Franck−Condon simulations in closer agreement to the experiment. Considerable improvement would be gained by including excitation operators for out-of-plane distortions along the amine hydrogen out-of-plane and in-plane bend coordinates and around the C−O bond. Nonetheless, the reasonable agreement between the experimental R2PI spectrum and the Franck−Condon simulations obtained with this strategy suggests that unlike other nucleic acids such as adenine[38] or cytosine,[39] and the remaining tautomers of guanine, the S_1 potential energy surface of the enol N7H tautomer is not affected significantly by anharmonicity (at least within the energy window investigated here), and we can furthermore conclude that for this particular tautomer any conical intersections otherwise involved in S_1 state lifetime-shortening relaxation processes, must occur at elevated energies.

The inability of the Franck−Condon simulations to faithfully reproduce the R2PI spectra of the remaining guanine tautomers (aside from inaccuracies in the calculated equilibrium structures) indicates that they possess significantly anharmonic S_1 potential energy surfaces and that here a more generalized approach has to be employed for the evaluation of the vibronic integrals. The inclusion of anharmonicities caused by CIs into vibronic simulations is an emerging field of research, and successful mathematical strategies have only recently been published.[40,41] The difference in spectral behavior between the enol N7H and the remaining tautomers of guanine underlined by the calculations and simulations presented in this work, furthermore, provides evidence that S_1 state lifetimes of DNA bases and associated relaxation processes are tautomer-specific, thus indicating, as already suggested in ref 42 the necessity for future time-resolved picosecond/femptosecond studies on these molecules to be able to discriminate between tautomers if a clearer picture of the S_1 state dynamics is to be gained.

Acknowledgment. The authors thank the EPSRC for funding part of the work (Grant No. GR/M48451/01) presented. Special thanks go to Dr. M. J. Watkins and Dr. M. C. R. Cockett for the inspiring discussions, useful comments, and suggestions made in the editing process of this manuscript. I.P. expresses his gratitude and thanks to his parents for financial support in the final writing stages of the manuscript.

Supporting Information Available: Figure showing the complete experimental R2PI spectrum of guanine labeling bands A−D; tables listing natural populations of the active space orbitals employed in the various CASSCF wave functions, and tables listing all CASSCF harmonic frequencies; Franck−Condon simulations of the enol N7H and enol N9H tautomers obtained from HF/CIS/cc-pVDZ geometries and normal modes; an expanded analysis of the Franck−Condon simulations of the enol N7H tautomer including the development of a uniform normal-mode nomenclature, the Duschinsky matrixes, and a detailed description of the simulations obtained from CIS and CASSCF equilibrium geometries; a figure showing the simulated tautomer-specific S_1–D_0 ZEKE/MATI spectra of guanine obtained from CASSCF-optimized geometries and frequencies. This material is available free of charge via the Internet at http://pubs.acs.org.

References and Notes

(1) Robertson, E. G.; Simons, J. P. *Phys. Chem. Chem. Phys.* **2001**, *3*, 1.

(2) Chin, W.; Mons, M.; Dognon, J.-P.; Piuzz, F.; Tardivel, B.; Dimicoli, I. *Phys. Chem. Chem. Phys.* **2004**, *10*, 2700.

(3) Nir, E.; Janzen, Ch.; Imhof, P.; Kleinermanns, K.; de Vries, M. S. *Phys. Chem. Chem. Phys.* **2002**, *4*, 732.

(4) Nir, E.; Janzen, Ch.; Imhof, P.; Kleinermanns, K.; de Vries, M. S. *Phys. Chem. Chem. Phys.* **2002**, *4*, 740.

(5) Nir, E.; Hünig, I.; Kleinermanns, K.; de Vries, M. S. *Phys. Chem. Chem. Phys.* **2003**, *5*, 4780.

(6) Nir, E.; Imhof, P.; Kleinermanns, K.; de Vries, M. S. *J. Am. Chem. Soc.* **2000**, *122*, 8091.

(7) Nir, E.; Hünig, I.; Kleinermanns, K.; de Vries, M. S. *Chem. Phys. Chem.* **2004**, *5*, 131.
(8) Bakker, J. M.; Compagnon, I.; Meijer, G.; Helden, G. v.; Kabeláč, M.; Hobza, P.; de Vries, M. S. *Phys. Chem. Chem. Phys.* **2004**, *6*, 2810.
(9) Schumm, S.; Gerhards, M.; Kleinermanns, K. *J. Phys. Chem. A* **2000**, *104*, 10648.
(10) Spangenberg, D.; Imhof, P.; Kleinermanns, K. *Phys. Chem. Chem. Phys.* **2003**, *5*, 2505.
(11) Pugliesi, I.; Müller-Dethelfs, K. *J. Phys. Chem. A* **2006**, *110*, 4657.
(12) Pugliesi, I.; Watkins, M. J.; Müller-Dethelfs, K. *J. Phys. Chem. A* **2006**, *110*, 4668.
(13) Nir, E.; Janzen, Ch.; Imhof, P.; Kleinermanns, K.; de Vries, M. S. *J. Chem. Phys.* **2001**, *115*, 4604.
(14) Piuzzi, F.; Mons, M.; Dimicoli, I.; Tardivel, B.; Zhao, Q. *Chem. Phys.* **2001**, *270*, 205.
(15) Mons, M.; Dimicoli, I.; Piuzzi, F.; Tardivel, B.; Elhanine, M. *J. Phys. Chem. A* **2002**, *106*, 5088.
(16) Petke, J. D.; Maggiora, G. M.; Christoffersen, R. F. *J. Am. Chem. Soc.* **1990**, *112*, 5452.
(17) Fulscher, M. P.; Serrano-Andres, L.; Roos, B. O. *J. Am. Chem. Soc.* **1997**, *119*, 6168.
(18) Langer, H.; Doltsinis, N. L. *J. Chem. Phys.* **2003**, *118*, 5400.
(19) Callis, P. R.; Vivian, J. T.; Slater, L. S. *Chem. Phys. Lett.* **1995**, *244*, 53.
(20) Seefeld, K. A.; Plützer, Ch.; Löwenich, D.; Häber, T.; Linder, R.; Kleinermanns, K.; Tatchen, J.; Marian, Ch. M. *Phys. Chem. Chem. Phys.* **2005**, *7*, 3021.
(21) Doktorov, E. V.; Malkin, I. A.; Man'ko V. I. *J. Mol. Spectrosc.* **1976**, *64*, 359.
(22) Ismail, N.; Blancafort, L.; Olivucci, M.; Kohler, B.; Robb, M. A. *J. Am. Chem. Soc.* **2002**, *124*, 6818.
(23) MOLPRO, version 2002.6, a package of ab initio programs designed by Werner, H.-J. and Knowles, P. J. with contributions from Amos, R. D.; Bernhardsson, A.; Berning, A.; Celani, P.; Cooper, D. L.; Deegan, M. J. O.; Dobbyn, A. J.; Eckert, F.; Hampel, C.; Hetzer, G.; Korona, T.; Lindh, R.; Lloyd, A. W.; McNicholas, S. J.; Manby, F. R.; Meyer, W.; Mura, M. E.; Nicklass, A.; Palmieri, P.; Pitzer, R.; Rauhut, G.; Schütz, M.; Schumann, U.; Stoll, H.; Stone, A. J.; Tarroni, R.; Thorsteinsson, T.
(24) Frisch, M. J.; Trucks, G. W.; Schlegel, H. B.; Scuseria, G. E.; Robb, M. A.; Cheeseman, J. R.; Montgomery, J. A.; Vreven, T., Jr.; Kudin, K. N.; Burant, J. C.; Millam, J. M.; Iyengar, S. S.; Tomasi, J.; Barone, V.; Mennucci, B.; Cossi, M.; Scalmani, G.; Rega, N.; Petersson, G. A.; Nakatsuji, H.; Hada, M.; Ehara, M.; Toyota, K.; Fukuda, R.; Hasegawa, J.; Ishida, M.; Nakajima, T.; Honda, Y.; Kitao, O.; Nakai, H.; Klene, M.; Li, X.; Knox, J. E.; Hratchian, H. P.; Cross, J. B.; Bakken, V.; Adamo, C.; Jaramillo, J.; Gomperts, R.; Stratmann, R. E.; Yazyev, O.; Austin, A. J.; Cammi, R.; Pomelli, C.; Ochterski, J. W.; Ayala, P. Y.; Morokuma, K.; Voth, G. A.; Salvador, P.; Dannenberg, J. J.; Zakrzewski, V. G.; Dapprich, S.; Daniels, A. D.; Strain, M. C.; Farkas, O.; Malick, D. K.; Rabuck, A. D.; Raghavachari, K.; Foresman, J. B.; Ortiz, J. V.; Cui, Q.; Baboul, A. G.; Clifford, S.; Cioslowski, J.; Stefanov, B. B.; Liu, G.; Liashenko, A.; Piskorz, P.; Komaromi, I.; Martin, R. L.; Fox, D. J.; Keith, T.; Al-Laham, M. A.; Peng, C. Y.; Nanayakkara, A.; Challacombe, M.; Gill, P. M. W.; Johnson, B.; Chen, W.; Wong, M. W.; Gonzalez, C.; Pople, J. A. *Gaussian 03*, revision C.01; Gaussian, Inc.: Wallingford, CT, 2004.
(25) Florian, J.; Leszczynski, J. *J. Am. Chem. Soc.* **1996**, *118*, 3010.
(26) Hobza, P.; Šponer, J. *Chem. Rev.* **1999**, *99*, 3247.
(27) Shukla, M. K.; Leszczynski, J. *Computational Chemistry: Reviews of Current Trends*; Leszczynski, J., Ed.; World Scientific: 2003; Vol. 8, Chapter 6, p 249.
(28) Chen, H.; Li, S. *J. Chem. Phys.* **2006**, *124*, 154315.
(29) Chin, W.; Mons, M.; Piuzzi, F.; Tardivel, B.; Dimicoli, I.; Gorb, L.; Leszczynski, J. *J. Phys. Chem. A* **2004**, *108*, 8237.
(30) Hanus, M.; Ryjáček, F.; Kabeláč, M.; Kubař, T.; Bogdan, T. V.; Trygubenko, S. A.; Hobza, P. *J. Am. Chem. Soc.* **2003**, *125*, 7678.
(31) Broo, A.; Holmén, A. *J. Phys. Chem. A* **2002**, *106*, 5088.
(32) Berden, G.; Meerts, W. L.; Jalviste, E. *J. Chem. Phys.* **1995**, *103*, 9596.
(33) Chin, W.; Mons, M.; Dimicoli, I.; Piuzzi, F.; Tardivel, B.; Elhanine, M. *Eur. Phys. J. D* **2002**, *20*, 347.
(34) Marian, C. M. *J. Chem. Phys.* **2005**, *122*, 104314.
(35) Kang, H.; Lee, K. T.; Jung, B.; Ko, Y. J.; Kim, S. K. *J. Am. Chem. Soc.* **2002**, *124*, 12958.
(36) Crews, B.; Abo-Riziq, A.; Grace, L.; Callahan, M.; Kabeláč, M.; Hobza, P.; de Vries, M. S. *Phys. Chem. Chem. Phys.* **2005**, *7*, 3015.
(37) Lee, K. T.; Sung, J.; Lee, K. J.; Kim, S. K.; Park, Y. D. *J. Chem. Phys.* **2002**, *116*, 8251.
(38) Plützer, Chr.; Kleinermanns, K. *Phys. Chem. Chem. Phys.* **2002**, *4*, 4877.
(39) Nir, E.; Müller, M.; Grace, L. I.; de Vries, M. S. *Chem. Phys. Lett.* **2002**, *355*, 59.
(40) Borrelli, R.; Peluso, A. *J. Chem. Phys.* **2003**, *119*, 8437.
(41) Kallush, S.; Segev, B.; Sergeev, A. V.; Heller, E. J. *J. Phys. Chem. A* **2002**, *106*, 6006.
(42) Ullrich, S.; Schultz, T.; Zgiersky, M. Z.; Stolow, A. *Phys. Chem. Chem. Phys.* **2004**, *6*, 2798.